Article

Silanization of Sapphire Surfaces for Optical Sensing Applications

Tanja Sandner, Annina M. Steinbach, Peter Knittel, Thomas Diemant, R. Jürgen Behm, Steffen Strehle, Christine Kranz, and Boris Mizaikoff

ACS Sens., **Just Accepted Manuscript** • DOI: 10.1021/acssensors.6b00786 • Publication Date (Web): 14 Mar 2017

Silanization of Sapphire Surfaces for Optical Sensing Applications

Tanja Sandner;[†;‡] Annina M. Steinbach;[§,‡] Peter Knittel,[†] Thomas Diemant,[‖] R. Jürgen Behm,[‖] Steffen Strehle,[§] Christine Kranz,[†] Boris Mizaikoff [*,†]

[†]Institute of Analytical and Bioanalytical Chemistry, Ulm University, Albert-Einstein-Allee 11, D-89081 Ulm, Germany

[§]Institute of Electron Devices and Circuits, Ulm University, Albert-Einstein-Allee 45, D-89081 Ulm, Germany

[‖]Institute of Surface Chemistry and Catalysis, Ulm University, Albert-Einstein-Allee 47, D-89081 Ulm, Germany

KEYWORDS: sapphire, self-assembled layers, binding properties, infrared reflection absorption spectroscopy, X-ray photoelectron spectroscopy, atomic force microscopy

ABSTRACT: Well characterized silane layers are essential for optimized attachment of (bio)molecules enabling reliable chem/bio sensor performance. Herein, binding properties and orientation of 3-mercaptopropyltrimethoxy silane layers at crystalline sapphire (0001) surfaces were determined by water contact angle measurements, infrared reflection absorption spectroscopy, atomic force microscopy, and X-ray photoelectron spectroscopy. Infrared reflection absorption spectroscopy measurements suggest an almost perpendicular arrangement of the MPTMS molecules to the substrate surface. Adhesion force studies between a silicon nitride AFM tip and modified sapphire, gold and silicon dioxide substrates were investigated by peak force tapping atomic force microscopy and used to define the silane binding properties on these surfaces. As expected, the Al-O-Si bond was determined to be responsible for the layer formation at the sapphire substrate surface.

Self-assembled monolayers (SAMs) are a simple yet reproducible method for surface modification providing an anchoring architecture for attaching, e.g., biological receptors, biomarkers or labels, which is especially important for biosensors.[1] Throughout the last decades, also the formation of SAMs on other surfaces as copper, palladium, and silver has become more prevalent, compared to the well-established silicon and gold surfaces.[2,3] All of these surfaces are commonly used as transducer materials (e.g., electrodes, waveguides, etc.) in chemo- or biosensors. In recent years, transparent transducer materials for optical chem/bio sensing applications were increasingly adopted in the field of biosensing.[4] Potential applications in optical sensing using these materials include mid-infrared (MIR) sensors based on attenuated total reflection (ATR), and biosensors based on microsphere resonators relying on resonant wavelength shifts during binding of analytes.[5–8] In particular, fiber optic ATR sensors enable analyzing binding events in real time via concentration-dependent attenuation of the evanescent field emanating at the interface between the optically denser waveguide made e.g., from sapphire, and an optically thinner medium such as an aqueous analyte solution.[9] For fiber optics, glass, diamond, and sapphire are probably the most relevant optical transparent interfaces according to their accessible electromagnetic windows. Due to the limited stability of glass in harsh environments,[4] diamond and sapphire have emerged as preferred substrates under such conditions owing to their chemical stability and mechanical robustness.[10] Sapphire is of particular interest in optical sensing applications, as the material is significantly less costly compared to diamond at almost comparable chemical and mechanical stability, next to transparency in a spectral region ranging from 200-5000 nm.[11] This optical window particularly facilitates monitoring C-H, N-H, and OH stretching vibrations.[7] Finally, sapphire may even be drawn into optical fibers, thus facilitating fiberoptic chem/bio sensing scenarios.[12,13] However the sensitivity towards special analytes could be enhanced by chemically modification of the sapphire fiber.[9] Despite its advantageous properties, there were few reports so far on the chemical surface modification of sapphire substrates,[14–16] and specifically on their silanization.[17–21] A homogenous silane layer at the optical transducer benefits the generation of binding sites for the immobilization of molecular recognition architectures, and to avoid scattering losses.[22] The silane layer should therefore ideally provide accessible binding moieties, while at the same time minimizing non-specific binding. Since the silanization procedure is critical to providing a well-controlled immobilization architectures, detailed control and characterization of this step is essential.[23] A uniform silane layer with high density facilitates diffusion limited binding, and positively affects further binding of, e.g., bioreceptors to this interface layer.[24-26] In the present study, we present and discuss a facile modification procedure for silanizing sapphire surfaces, along with a study on the binding behavior of alkylsilanes at sapphire (0001) surfaces. Furthermore, the orientation of the alkylsilanes in the obtained layer at the surface was investigated for optimizing the attachment of biomolecules at these substrates enabling advanced chem/bio sensing.[27]

EXPERIMENTAL SECTION

Sapphire wafers (c-plane, double side polished, roughness $R_a \leq 0.3$ nm) were obtained from Hi-solar (Daechon-dong, Korea). Acetone and 2-propanol (VLSI grade) for substrate cleaning were obtained from Technic (Saint Denis, France). 3-Mercaptopropyltrimethoxysilane (MPTMS, 95 %), and dodecanthiol (DDT, 98 %) were purchased from Alfa Aesar (Karlsruhe, Germany) and used as received. Sulfuric acid (95 %) and hydrogen peroxide (30 %) were obtained from VWR Chemicals (Bruchsal, Germany) and Merck Millipore (Darmstadt, Germany), respectively. Aqueous solutions were prepared with ultrapure water, conductivity 18.3 MΩ with Milli-Q academic (Merck Millipore, Darmstadt, Germany). Argon 4.6 was purchased from MTI IndustrieGase AG (Neu-Ulm, Germany).

Substrate preparation. Micropatterned substrates were produced on a bare sapphire surface (0001, c-plane) by depositing a layer (100 nm) of silicon dioxide using plasma enhanced chemical vapor deposition (Oxford Plasmalab PE-CVD, Oxford Instruments, Wiesbaden, Germany), followed by e-beam lithography (Leica EBPG 5 HR, Leica Microsystems, Jena, Germany), and HF etching for structuring the SiO_2 layer, yielding the first segment of the pattern (i.e., 'flower-shaped petals'). The gold surface in the middle of the pattern (figure 4) was obtained via e-beam lithography and subsequent deposition of a Ti/Au layer by thermal evaporation (Edwards Temescal FC-1800, Ferro Tec, München, Germany) with a total thickness of 50 nm, followed by a lift-off procedure. The substrate was further cleaned by ultrasonification in acetone and 2-propanol for 5 min each, and then dried in a nitrogen stream. The substrate surface was activated via plasma treatment (100 W/100 torr O_2/10 min) (Plasmalab µ-etch, Oxford Instruments, Wiesbaden, Germany), rendering the surface hydrophilic for the subsequent modification.

Gas phase silanization. The micropatterned as well as bare sapphire substrates were silanized using a gas phase deposition device specifically tailored for silanization.[28] 350 µl MPTMS were loaded into the reaction device and an argon stream was guided through the liquid silane reservoir. The argon stream then passes the substrate, allowing evaporated silane to react with and deposit onto the substrate surface. For a reaction time of 1 h, the argon flow was set to approximately 5 L/h. After the reaction, the substrate was rinsed with 2-propanol and dried in an argon stream.

Silanization by immersion. For silanization procedures in liquid, sapphire substrates were cleaned for 10 min in piranha solution (caution: Piranha solution interacts strongly with organic compounds and needs to be handled with extreme caution!) (3:1, sulfuric acid: hydrogen peroxide), extensively rinsed in DI water, and dried in an argon stream. For the self-assembling, the sapphire substrates were immersed in 1 mM dodecanthiol dissolved in 2-propanol solution for 20 h. After the reaction, the modified substrates were successively cleaned in an ultrasonic bath with 2-propanol, and dried in an argon stream.

Contact angle. Water contact angles were measured using a Dataphysics OCA 15 Pro contact angle system (DataPhysics, Filderstadt, Germany) and a SCA20 analyzer using the sessile drop (needle-in) method. Here, the quasi-static water contact angles at three different spots per sample were obtained.

IRRAS. Infrared reflection absorption spectroscopy (IRRAS) was performed using with a Bruker Vertex 70 spectrometer (Bruker Optics, Ettlingen, Germany) equipped with an A513/Q angle grazing unit and a motorized polarizer holder A121. For each IR spectrum, 500 scans at a spectral resolution of 4 cm^{-1} in the range of 4000-400 cm^{-1} were averaged. Spectra at various angles of incidence between the surface normal and the IR beam, were measured. Additionally, differently polarized light (s- and p-polarized) was used at each angle of incidence. A cleaned blank sapphire substrate was used as background sample for determining the absorbance value following $A = -\log (R/R_0)$ where R is the reflectivity of the modified layer on sapphire and R_0 is the reflectivity of a bare sapphire substrate.

AFM. Atomic force microscopy (AFM) measurements were carried out using a BrukerBioScope Catalyst system (Bruker Optics, Ettlingen, Germany). Silicon nitride probes (DNP-A, $f_0 = 65$ kHz, Bruker Nano Analytics, Karlsruhe, Germany) with a nominal spring constant of 0.35 N/m were used. All measurements were performed in aqueous solution (0.1 mol/L KCl) using the peak force tapping mode (peak force: 3 nN, oscillation frequency: 1 kHz) at ambient conditions. For data evaluation, the NanoScope Analysis Software was used.

XPS. X-ray photoelectron spectroscopy (XPS) measurements were performed with a PHI 5800MultiTechnique ESCA System (Physical Electronics, Eden Prairie, USA) using monochromatized Al K_α radiation (1486.6 eV). Each substrate was analyzed at take-off angles of 20° and 45° with respect to the surface by recording survey scans (pass energy: 93.3 eV, step width: 0.4 eV and high-resolution scans of the peaks of interest (29.35 eV and 0.125 eV increments). The data were analyzed via the OriginPro9G software package and the Shirley background correction was used. The bare sapphire substrate was used as internal standard, i.e., the binding energy scale was calibrated to the Al 2p peak for Al_2O_3 at 74.1 eV.

RESULTS AND DISCUSSION

The application of sapphire substrates for optical biosensors requires the modification of the transducer surface via an appropriate interface, e.g., a silane layer that facilitates a controlled immobilization of bioreceptors. Therefore, plane sapphire (0001) slides were modified with MTPMS using a gas phase deposition system previously described by our research team.[28] The modified sapphire substrates were then used for detailed surface analysis including contact angle measurements, IR reflection absorption spectroscopy, and XPS measurements. Additionally, micropatterned sapphire substrates with structures composed of silicone dioxide and gold were investigated via AFM measurements in a peak force tapping mode.

Contact angle measurements. For a first evaluation of MPTMS modified sapphire substrates, water contact angles were determined. Prior to the modification procedure, the substrates were rinsed with acetone and 2-propanol, and then subjected to plasma surface treatment (10 min in oxygen plasma, 100 W, 100 Torr). As anticipated, sapphire substrates treated this way showed a water contact angle of 15±1°. The determined contact angle fits very well to values described in the literature, and indicates a pronounced surface hydrophilicity due to prevalent surface hydroxyl groups.[11] Modifying a sapphire

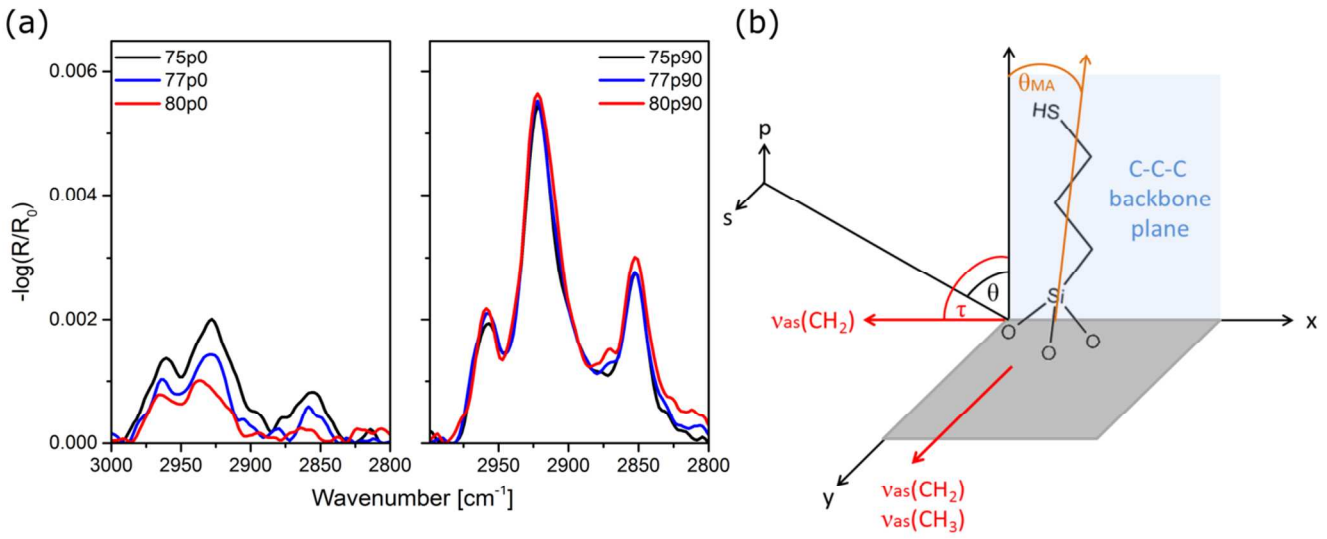

Figure 1. (a) Baseline corrected IRRAS spectra of the CH_2 groups associated with the propylic chain of the organosilane determined at three different incident angles, and via illumination with s-polarized (left) and p-polarized (right) IR radiation, respectively. (b) Scheme of the MPTMS molecule orientation on the sapphire surface and their transition dipole moment vectors (red arrows).

substrate with MPTMS via the gas phase deposition routine described above yields a contact angle of approx. 58±3°. For the silicon dioxide modification with MPTMS, we measured a value of 50±3°.[28] For comparison, contact angle values for MPTMS reported in literature are ranging from 53-58°, which are also in good agreement to our data.[29–31] The obtained results suggest that the surface modification via MPTMS deposition was successful, due to comparable hydrophilicity of the modified surfaces. The similar contact angle values for modified sapphire and silicon dioxide surfaces indicate that the chemical groups on top of the layer should be similar. From the contact angle measurements, it can therefore just be concluded that hydrophilic sapphire substrates apparently react analogously to oxidized silicon surfaces. Nevertheless, this presumption needs to be proven by further detailed characterization via IR, XPS, and AFM studies.

Infrared spectroscopy. To further elucidate the presence and nature of the MPTMS layer attachment, and to potentially obtain information on the molecular orientation in the layer, we performed IRRAS measurements using polarized IR radiation. Due to the rather weak absorbance of MPTMS layers, the -CH_2- vibration band as the most pronounced IR signature was evaluated. Planar MPTMS-modified sapphire substrates were analyzed in reflection absorption mode[32–34] at two different polarization states (i.e., p90 corrsp. to p-polarized IR radiation, and p0 corresp. to s-polarized IR radiation). Furthermore, different angles of incidence vs. the surface normal were investigated (i.e., 75-80 deg). Figure 1a shows characteristic absorption bands attributed to the propylic chain of MPTMS at s- and p-polarized illumination. The bands located at 2922 cm^{-1} and 2852 cm^{-1} are assigned to the asymmetric $\nu_a(CH_2)$ and symmetric $\nu_s(CH_2)$ stretching vibrations of the CH_2 groups of the propylic chain associated with the organosilane, respectively.[35] The peak emerging at a wavelength of 2956 cm^{-1} was assigned to the asymmetric $\nu_a(CH_3)$ vibration of the methoxy group. This band arises from silane groups that are not completely hydrolyzed and crosslinked.[30] As noted by Porter et al the peak position strongly depends on the alkyl chain length.[36] The location of peak increase as the length of the alkyl chain decreases. For short alkyl chains (n=5) peak positions of 2921 cm^{-1} are reported, whereas longer alkyl chains like n=21 revealed peak positions of 2918 cm^{-1}. The measured band of 2922 cm^{-1} for the asymmetric CH_2 stretching vibration confirms the correlation between the alkyl chain length and the peak position. The S-H stretch vibrations are not observed due to low absorption coefficient.[30]

The IRRAS method is particularly useful in studying the orientation of the adsorbed molecules, derived from the peak direction. For adsorbed molecules on dielectric substrates, e.g. as the sapphire, the band intensities and orientation of the absorbance strongly depend on the polarization of the IR beam, the reflectivity of the substrate, before and after the modification, the refractive index, the Brewster angle and the orientation of the transition dipole moment vector.[32,33,37–39] For c-plane sapphire, the refractive index is, depending on the wavelength, approx. 1.7 and the Brewster angle is approx. 60 deg.[40,41] Therefore it is important to note that all measured incidence angles (defined as the angle between the central ray and the surface normal, θ) are greater than the Brewster angle of 60 deg. Furthermore, we make the assumption that the chain axis is straight and not twisted, due to the short chain length. On dielectric substrates, s-polarized radiation (p0) only probes the dipole moment vectors parallel to the surface.[32] Figure 1b displays the important components contributing to the peak absorption. The incidence angle of the radiation is described by θ, and the transition dipole vectors are defined by τ, the transition dipole moment tilt angle. θ_{MA} depict the molecular tilt angle, measured from the molecular axis to the surface normal. On the assumption that our short MPTMS molecule is oriented close to the surface normal, the vectors of the transition dipole moments for the $\nu_a(CH_2)$, $\nu_s(CH_2)$ and $\nu_a(CH_3)$ stretching modes are perpendicular to the molecular axis (figure 1b).[37] Further, the transition dipole moment $\nu_s(CH_2)$ is oriented parallel to the C-C-C plane, formed by the C-C-C backbone. While the transition dipole moment vectors $\nu_a(CH_2)$, $\nu_a(CH_3)$ are oriented perpendicular towards the C-C-C plane.[37] Hence, the s-polarized spectra are dominated by the $\nu_a(CH_2)$, $\nu_s(CH_2)$ and $\nu_a(CH_3)$ bands with their dipole

moments oriented parallel to the surface, enabling interaction with s-polarized light (figure 1b). Previous studies have reported that τ, the angle that defines the transition dipole moment vector, ranges between 80-90 deg. for all stretching modes.[32,38] These large angles permit a great interaction with the electric field of the s-polarized radiation. Resulting, the peak intensities of the three stretching vibrations can be seen in the s-polarization.

The band intensities for the s-polarization, shown in figure 1a, decrease with increasing incidence angle. This behavior is known for s-polarized radiation due to the increasing reflectivity of the substrate after the modification.[32] On dielectric substrates, negative absorbances are expected for all incidence angles.[32,42] Surprisingly, the peak absorptions for the s-polarization, shown in figure 1a, are positive. However, carbonic residual intensities remain as a positive absorbance.[34,42] P-polarization, which probes transition dipole moment vectors parallel and perpendicular to the surface, yields strong positive absorption of all three stretching modes caused by the strong interaction with the electric field parallel to the surface (figure 1a).[32] For measurements above the Brewster angle and at high τ angles, positive bands are expected.[32] Hence, the results obtained here agree with the theoretically anticipated behavior described in the literature.[32] In the case of a lying MPTMS molecule, assuming no changes in the tilt angle the orientation of the transition dipole moment vectors of the $\nu_a(CH_2)$, $\nu_a(CH_3)$ would be equal but the vector of $\nu_s(CH_2)$ would point in z-direction. The band of $\nu_s(CH_2)$ would cause negative absorbance due to the interaction with the electric field perpendicular to the surface. However, the orientation of the bands and intensities at p-polarized illumination conditions suggest that the chain axis is oriented close to the surface normal.

Unfortunately, the peak orientation and intensities would react similar for an isotropic MPTMS layer. In an isotropic layer the molecule orientations are distributed randomly and therefore each transition dipole moment vector assumes the same average distribution defined by a tilt angle of 54.7°. With its either low refractive index of 1.7, mainly the electric field parallel to the surface is responsible for the absorption.[32] Due to the fact, that this component is positive at incidence angles higher than the Brewster angle, it may be possible that the layer is isotropic. For an isotropic layer, rather small intensities of 0.000-0.0002[32] are expected. We observed higher values, which are assumed for anisotropic films. This point therefore suggests an anisotropic layer formation. However, an anisotropic film of our short MPTMS is surprising because it is known that decreasing the alkyl chain length results in the formation of a less densely packed structure.[36]

The obtained IRRAS results not only provide evidence for the presence of MPTMS on sapphire substrates after a gas phase deposition, but in addition may indicate an almost perpendicular orientation of the short-chained MPTMS molecules at the sapphire substrate surface. Nevertheless, a quantitative determination of the molecule orientation requires a spectral simulation.

XPS measurements. Contact angle measurements and IRRAS studies indicated a successful surface modification, yet more information is required on the actual binding situation, e.g., which fiunctionality of the silane (i.e., the methoxy- or thiol-group) is reacting with the sapphire surface. Therefore, X-ray photoelectron spectroscopy measurements were performed to investigate the binding situation between the mercaptosilane and the sapphire substrate surface. In the survey spectra, shown in figure 2, the presence of alumina and oxygen is attributed to the sapphire substrate. The appearance of silicon, carbon and sulfur can be attributed to the mercaptosilane.

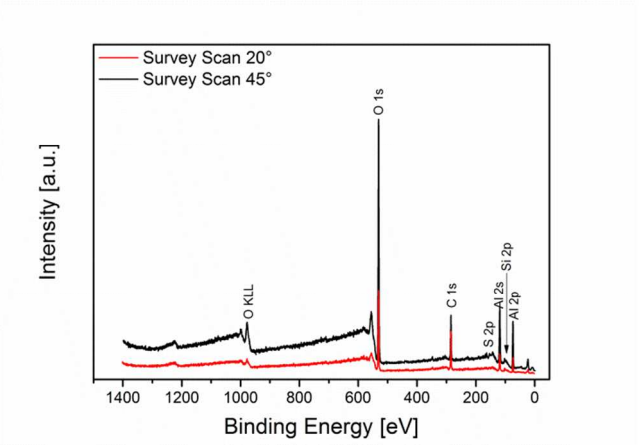

Figure 2. Survey spectra of sapphire substrate modified with MPTMS at different take-off angles.

In order to evaluate changes in the binding situation high resolution peaks of Al 2p, O 1s, Si 2p and the S 2p after the gas phase MPTMS modification were examined at take-off angles of 20° and 45° with respect to the surface. For all results shown herein, the binding energy scale was calibrated to the Al 2p peak for sapphire at 74.1 eV.[43,44] In addition, a Shirley background correction was used and the fitting function of the Origin Software, which used a combination of Gaussian as well as Lorentzian components, was applied. The high-resolution spectra of Al 2p at a take-off angle of 45° (figure 3) reveal a symmetric peak (R^2 = 0.996) at a binding energy of 74.1 eV. At the surface sensitive take-off angle of 20° the barely visible asymmetric peak can be fitted with two contributions around 74 - 75 eV (R^2 = 0.998). The Al 2p signal is slightly shifted to higher binding energy as part of the MPTMS binds to the sapphire surface.

The spectra of the O 1s peak changed visibly from a take-off angle of 45° to 20°. At 45° the peak at 530.8 eV with a FWHM of 1.8 eV (R^2 = 0.983) is assigned to the Al-O bond in the α sapphire.[43,44] This position mainly reflects our sapphire substrate. The O 1s peak becomes asymmetric and broad at a take-off angle of 20° and can be fitted with four components (R^2 = 0.993) corresponding to different states of the oxygen. The peaks at 530.4-530.8 eV are still shifted to higher binding energies. The component at 531.7 eV is mainly attributed to the Si-O-Al bonds.[45,46] This peak firstly indicates a bond between silicon from the mercaptosilane to the oxygen of the sapphire substrate. Lastly, the peak around 532.0 eV is related to the presence of surface hydroxyl groups on the sapphire as it is expected after the cleaning procedure with oxygen plasma.[46] The broadening of the peak triggered by the chemical shift towards higher binding energies underlines changes in electron density on the oxygen atom effected by the self-assembly of the MPTMS. Compared to aluminum, silicon has a slightly higher electronegativity which explains the small shift in binding energies towards higher values. The peak shape of the Si 2p peak (R^2=0.950) remains similar regardless of the take-off angle. However, a shift of the peak maxima

towards higher binding energies is visible. The increase of the binding energies can be explained by the self-assembly of the MPTMS. These results support the assumption that the silanization takes place via a Si-O-Al bond and not via a bond between the sapphire and sulfur.

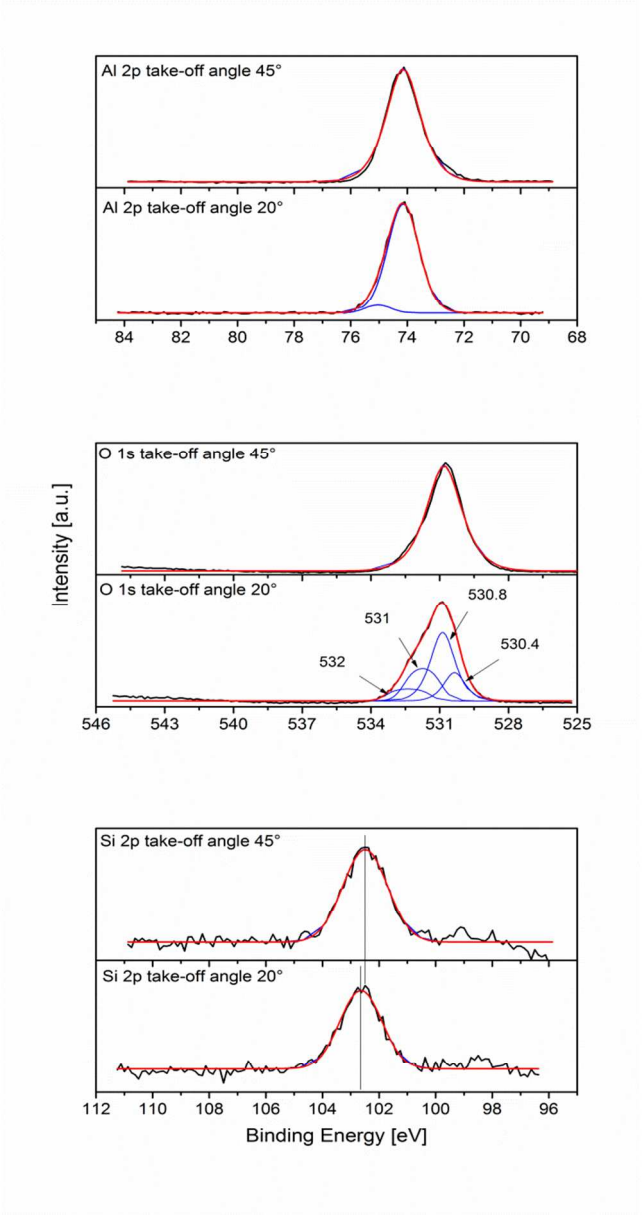

Figure 3. High-resolution XPS spectra with peak fit for the Al 2p peak, the O 1s and the Si 2p peak after the MPTMS deposition at a sapphire substrate surface. The fitted peaks are shown in blue and the cumulative pulse fit is shown as solid red line.

In contrast to aluminum, oxygen and silicon, no changes in binding energies or the peak shape can be found for carbon and sulfur according to the different take-off angles. Figure 4 exemplary illustrates high-resolution XPS spectra of the C 1s peak and the S 2p peaks. Both spectra of the C 1s peaks can be fitted (R^2=0.997) with one single contribution at 284.8 eV, denoting the C-C, C-Si and C-H peaks.[46–48] It should be noted that the C 1s signal might include some carbonaceous contaminant.

In order to rule out a chemical bonding between the sulfur or thiol group to the sapphire substrate it is more important to look closer at the S 2p peaks. At both angles, we observed two distinct peaks at binding energies of 169.0 and 163.5 eV, which were assigned to oxidized sulfur (i.e., -SOxH) species and reduced sulfur (i.e., SH, -SS-), respectively.[31,49,50] Since no obvious changes occurred in binding energies and peak shapes it seems that the sulfur is not involved in the binding process to the sapphire surface. Consequently, the data support the hypothesis that only the methoxy group is responsible for bonding organosilanes to the aluminum oxide/sapphire surface via an Al-O-Si bond.

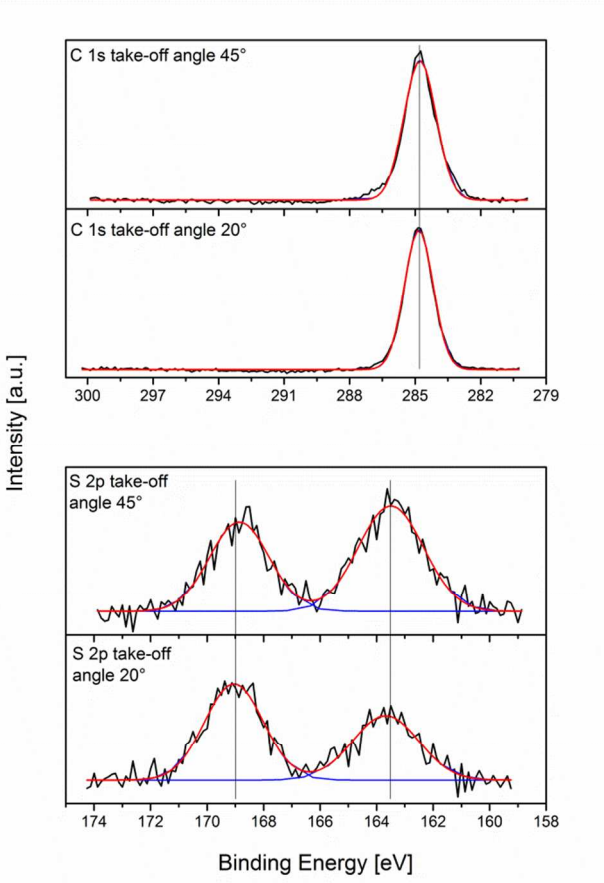

Figure 4. High-resolution XPS spectra with peak fit for the C 1s and S 2p peaks after the MPTMS deposition at a sapphire substrates surface at various take-off angles.

AFM studies. Finally, to directly compare the surface chemistry presented by the MPTMS layers when bound to sapphire, silicon dioxide, and gold, atomic force microscopy adhesion mapping was conducted at micropatterned sapphire substrates comprising silicon dioxide and gold features. Since the binding situation of silanes and thiols is well-known at gold and silicon dioxide surfaces, these materials have been selected as internal references. Furthermore, the self-assembly process at these surfaces is based on different reaction mechanism. SAMs at gold surfaces emerge from the formation of thiol-gold bonds,[51,52] while at silicon surfaces the siloxane groups of the oxidized - and therefore hydroxylated - silicon

surface react via condensation with the methoxygroups of the organosilanes.[55] Using accordingly patterned substrates, a direct comparison of the adhesion forces (i.e., either thiol or alkane groups) between the adsorbed layer and an AFM Si_3N_4 tip is facilitated. Accordingly, information whether the methoxy group or the thiol group is responsible for the layer formation may be obtained.

All AFM measurements were performed in electrolyte solution containing 1 mol/L KCl. Therefore, the presence of capillary forces is excluded as a cause for the change in the adhesion force, which efficiently screens the electrostatic forces. Figure 5 shows an optical image of the micropatterned sapphire substrate. The central hexagonal structure represents a gold pattern with a height of 50 nm (i.e., 5 nm Ti and 45 nm Au). The flower petal pattern comprises silicon dioxide with a thickness of 100 nm.

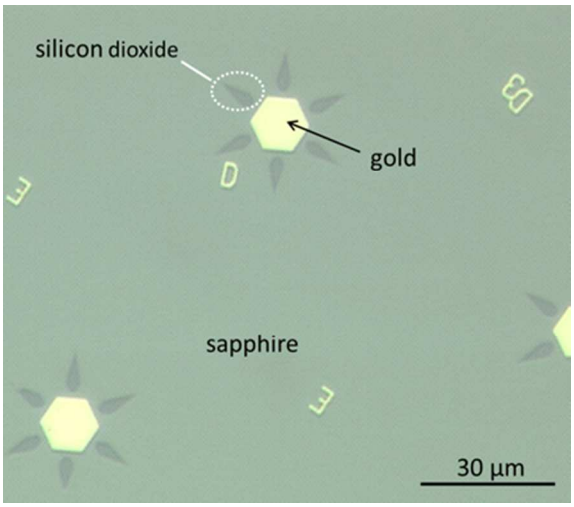

Figure 5. Optical image of the micropatterned sapphire substrate, comprising gold and silicon dioxide features.

To exclude a binding of thiol to the sapphire, the micropatterned surface was modified with dodecanthiol (DDT) and the average adhesion force between a silicon nitride (Si_3N_4, DNP, Bruker) AFM tip and the modified surfaces was determined. For this experiment the longer DDT molecule was used instead of the short MPTMS, because with such a short chain length we would be under the detection limit. Hence, a cleaned micropatterned sapphire substrate was immersed for 20 h in 1 mM DDT dissolved in ethanol.[56] The thiol group of the DDT molecule binds to the gold surface, forming a DDT self-assembled monolayer.[56] According to Ptak et al. this would result in a strong adhesive interaction between the Si_3N_4 AFM tip (Si_3N_4, MLCT-F, Veeco, USA) and the methylene groups of the DDT caused by van der Waals forces.[56] The sapphire substrate and the silicon dioxide features lack of this specific thiol-gold interaction.[51,52] Consequently, only the formation of a physically adsorbed DDT layer with reduced adhesive interaction and no change in height is expected and observed (figure 6c, e). Reduced adhesive forces are expected for physically adsorbed layers because of the incomplete layer formation. Figure 6a, b and c summarize the obtained height profiles at bare (a) and at DDT modified sample surfaces (b). The line profile (white line figure 6b) of the height and adhesion differences before and after the DDT modification is shown in Figure 6c. No obvious difference in height is visible, which may be related to the surface roughness of the gold surface in a range of 3 nm (rms) taking into account that the self-assembled monolayer has only a height of 1.7 nm[57] and therefore the small height difference cannot be determined.

Figure 6d shows a representative 3D example of peak force tapping measurements on a micropatterned substrate after DDT modification including the simultaneously measured height and adhesion force information. Prior to the modification, no significant adhesion contrast between the individual features has been observed (Fig. 6c and e) This behavior can be explained by the fact that the substrate was cleaned and activated with piranha, thereby rendering the surfaces hydrophilic for the following modification step. In addition, the low set point of 3 nN and the AFM tip radius of 20 nm prevent a deeper penetration of the tip into the surface, which explains why the hydrophilic surfaces reveal similar adhesion forces. The adhesion forces measured prior to the modification were 0.039 ± 0.077 nN (N = 2400) for sapphire, 0.043 ± 0.066 nN (N = 5700) for gold, and 0.102 ± 0.055 nN (N = 5700) for silicon dioxide. The standard deviation for these small adhesion force values is evidently high, as the values are close to the detection limit of the method. Therefore, within the limits of the method, there are no apparent differences between the three surfaces prior to the modification.

However, after the DDT modification, the average adhesion force recorded at the gold feature appears significantly higher, increasing from 0.043 ± 0.066 to 4.44 ± 0.91 nN (N = 5700). The equally distributed increase in adhesion force on the gold surface confirms the successful DDT modification due to the strong adhesive interaction between the Si_3N_4 AFM tip and the hydrophobic DDT layer. These adhesive forces of approx. 4.44 nN between the tip and the methylene groups at the DDT modified gold feature surface, as observed in the force curves, are readily attributed to DLVO forces (DLVO named after Derjaguin, Landau, Verwey, Overbeek), which are a combination of double layer forces and van der Waals forces largely representing hydrophobic interactions.[58,59] Previous studies have indicated adhesive forces of approx. 15 nN in contrast to the 4.44 nN determined in this study.[56] Due to the effective radius of the AFM tip curvature, the higher loading rate and a decreased loading force, it was anticipated that the determined adhesive forces are lower in peak force tapping mode.

Only a slight increase of adhesion forces for sapphire and silicon dioxide after the DDT modification is observed. This increase may be caused by the formation physically adsorbed DDT layer characterized by a reduced adhesive interaction. Further indication for the physical adsorption is that the adhesive force values can be reduced for silicon and sapphire surfaces after sonication (data not shown). Compared to 1.20 ± 0.18 nN (N = 9180) at the sapphire surface, and 1.33 ± 0.26 nN (N = 1304) at the silicon dioxide structure, after the modification step the adhesion is approx. four-times higher for gold. Hence, sapphire and silicon dioxide reveal similar reduced adhesive interactions with the silicon nitride probe compared to the DDT-modified gold structure. The strong adhesion difference between sapphire and gold indicates that - similar to the situation on silicon dioxide DDT - is presumably not covalently bound to sapphire. These results further confirm the hypothesis that there are no covalent or semi-covalent chemical bonds between sulfur and the sapphire surface, which in turn corroborates that MPTMS bind via the Si-O-Al bond. Hence, MPTMS molecules bind via the methoxy

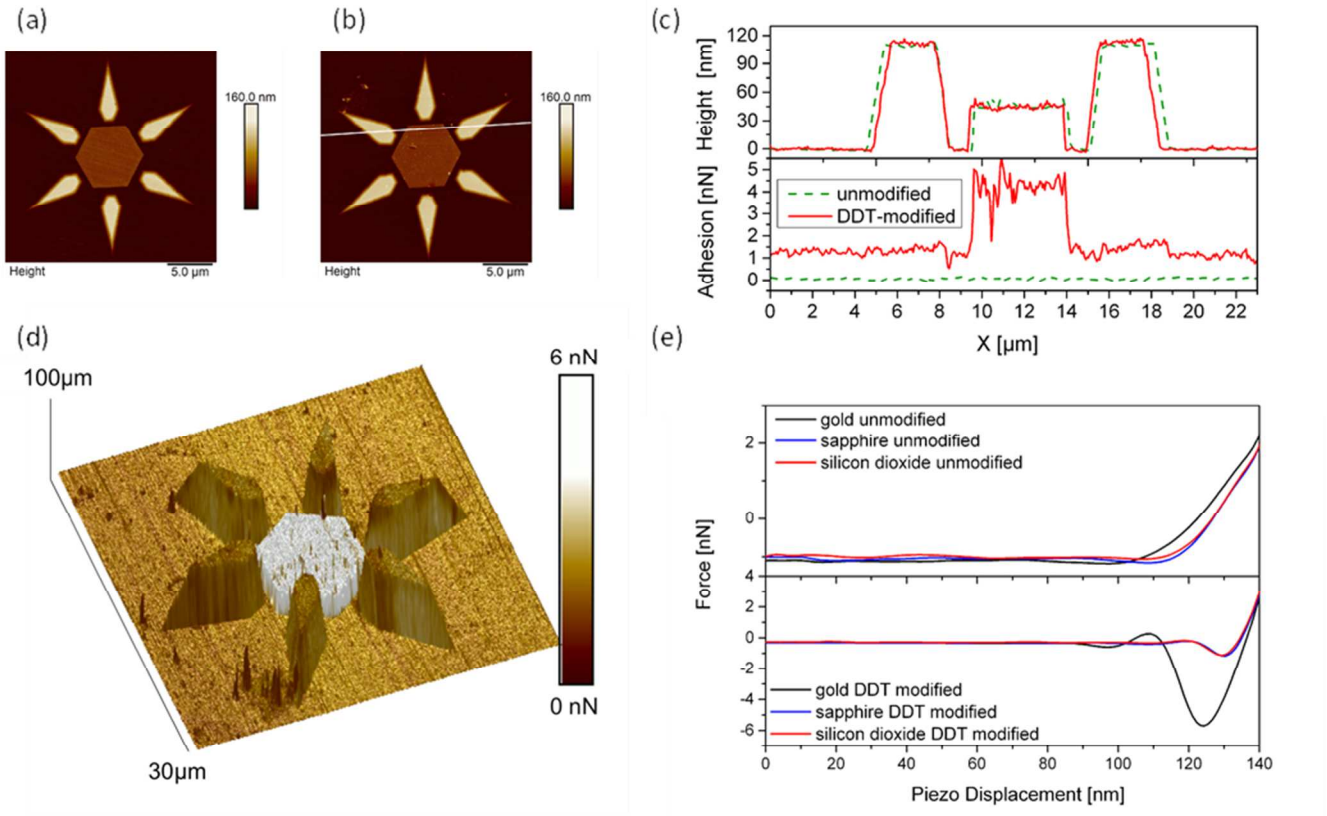

Figure 6. (a) Topography image before and (b) after the DDT modification. (c) Height and adhesion profiles of the unmodified and DDT modified micropatterned substrate. (d) 3D AFM topography image comprising the correlated adhesion force contract for each surface recorded in peak force tapping mode at a DDT-modified micropatterned sapphire substrate. (e) Corresponding force curves on the bare und DDT modified substrate (retract part) of gold (black), sapphire (blue), and silicon dioxide (red).

groups, and thus formed layers are not affected by thiol-sapphire interactions.

The results obtained via the individual characterization techniques confirm the successful modification of sapphire surfaces. The water contact angles were increased after the modification indicating a change of the hydrophilicity at the sapphire surface comparable to glass surfaces. While contact angle measurements provide information on macroscopic changes, XPS and IRRAS give more detailed insight into the surface chemistry. IRRAS studies characterize the functional groups present at the surface, and the spatial orientation of the silane molecules. Herein, next to a successful surface modification an almost perpendicular orientation of MTPMS molecules was confirmed. XPS gives details on the binding properties. Next to confirming the presence of the relevant elements, the obtained XPS results suggested that the methoxy group of the MTPMS is responsible for the layer formation at the sapphire surface, again corroborating similarities to glass surfaces. These findings are in agreement with the water contact angle measurements indicating similar hydrophilicity, and with the almost perpendicular molecular orientation derived from the IRRAS measurements. AFM studies on the adhesion forces between silicon dioxide, sapphire, and gold surfaces after modification with the thiolalkane DDT and a Si_3N_4 tip aid in excluding potential thiol-sapphire binding. Since the interaction between the hydrophobic DDT layer on gold and the AFM tip resulted in the highest adhesion forces vs. sapphire and silicone dioxide with similar adhesion force values it is evident that only the gold surface interacts with the DDT thiol group. Hence, the AFM studies complementarily support the obtained XPS results, i.e., that a chemisorbed layer was likely achieved via Si-O-Al bonds.

CONCLUSIONS

The binding situation along with the molecular orientation of MPTMS molecules deposited from the vapor phase at planar sapphire substrate surfaces were investigated. Self-assembled MPTMS layers were subsequently analyzed by water contact angle measurements, IRRAS using polarized IR radiation, XPS, and AFM peak force tapping measurements to derive adhesion forces. Each characterization technique provides complementary information on the binding situation at sapphire surfaces. Contact angle measurements confirmed a successful MPTMS deposition at the sapphire substrate surface by a change of the surface contact angle from 15±1° (hydrophilic) to 58±3° (hydrophobic). Corresponding XPS and IRRAS measurements confirmed the presence of MPTMS, and additionally suggested that MPTMS binds to the sapphire surface via the formation of silicon alkoxides resulting in Si-O-Al bonds, which apparently give rise to a nearly perpendicular

orientation of the MPTMS molecules in correlation to the substrate surface. To exclude sulfur-sapphire bonds, additional AFM adhesion force studies at three different surfaces (i.e., silicon dioxide, gold and sapphire) were done. In summary, these findings provide insight on the attachment of organosilanes at sapphire surfaces at a molecular level, and allow for the application of such interface architectures as versatile and tailorable immobilization layers for a wide variety of molecular recognition moieties required, e.g., for sapphire-based chem/bio sensors.

AUTHOR INFORMATION

Corresponding Author

* E-Mail: boris.mizaikoff@uni-ulm.de

Author Contributions

T.S., A.S., P.K., and T.D. contributed to the experiments discussed in this article. ‡These authors contributed equally.

ACKNOWLEDGMENT

This work was financially supported by the Federal Ministry of Research and Education, Germany (FKZ: 13N12545). The authors thank S. Jenisch for the experimental support and the glassblowers J. Geißel and J. Müller for producing the gas phase modification device.

REFERENCES

(1) Chaki, N. K.; Vijayamohanan, K. Self-Assembled Monolayers as a Tunable Platform for Biosensor Applications. *Biosens. Bioelectron.* **2002**, *17* (1–2), 1–12.

(2) Love, J. C.; Estroff, L. A.; Kriebel, J. K.; Nuzzo, R. G.; Whitesides, G. M. Self-Assembled Monolayers of Thiolates on Metals as a Form of Nanotechnology. *Chem. Rev.* **2005**, *105* (4), 1103–1169.

(3) Schoenfisch, M. H.; Pemberton, J. E. Air Stability of Alkanethiol Self-Assembled Monolayers on Silver and Gold Surfaces. *J. Am. Chem. Soc.* **1998**, *120* (18), 4502–5413.

(4) Murib, M. S.; Yeap, W. S.; Martens, D.; Liu, X.; Bienstman, P.; Fahlman, M.; Schöning, M. J.; Michiels, L.; Haenen, K.; Serpengüzel, A.; et al. Photonic Studies on Polymer-Coated Sapphire-Spheres : A Model System for Biological Ligands. *Sensors Actuators A Phys.* **2015**, *222*, 212–219.

(5) Mizaikoff, B. Mid-IR Fiber-Optic Sensors. *Anal. Chem.* **2003**, *75(11)*, 258A–267A.

(6) Vollmer, F.; Arnold, S. Whispering-Gallery-Mode Biosensing: Label-Free Detection down to Single Molecules. *Nat. Methods* **2008**, *5* (7), 591–596.

(7) Götz, R.; Mizaikoff, B.; Kellner, R. Application of Sapphire Fibers to an IR Fiber-Optic Sensor for the Investigation of Polymers at Elevated Temperature. *Appl. Spectrosc.* **1998**, *52* (9), 1248–1252.

(8) Murib, M. S.; Tran, A. Q.; De Ceuninck, W.; Schöning, M. J.; Nesladek, M.; Serpengüzel, A.; Wagner, P. Analysis of an Optical Biosensor Based on Elastic Light Scattering from Diamond-, Glass-, and Sapphire Microspheres. *Phys. Status Solidi Appl. Mater. Sci.* **2012**, *209* (9), 1804–1810.

(9) Mizaikoff, B.; Göbel, R.; Krska, R.; Taga, K.; Kellner, R.; Tacke, M.; Katzir, A. Infrared Fiber-Optical Chemical Sensors with Reactive Surface Coatings. *Sensors Actuators B. Chem.* **1995**, *29* (1–3), 58–63.

(10) Isono, T.; Ikeda, T.; Aoki, R.; Yamazaki, K.; Ogino, T. Structural- and Chemical-Phase-Separation on Single Crystalline Sapphire (0001) Surfaces. *Surf. Sci.* **2010**, *604* (21–22), 2055–2063.

(11) Takahashi, H.; Shirahata, N.; Narushima, T.; Yonezawa, T. Self-Assembly of Gold Nanoparticles on a Single Crystalline Sapphire Substrate. *Appl. Surf. Sci.* **2012**, *262*, 129–133.

(12) Mizaikoff, B.; Goetz, R.; Kellner, R. IR Fiber Optic Evanescent Field Sensors for Gas Monitoring. In *Proc. SPIE*; 1995; Vol. 2508, pp 253–264.

(13) Harrington, J. A. A Review of IR Transmitting, Hollow Waveguides. *Fiber Integr. Opt.* **2000**, *19* (3), 211–227.

(14) Lim, M.; Feng, K.; Chen, X.; Wu, N.; Raman, A.; Nightingale, J.; Gawalt, E.; Korakakis, D.; Hornak, L. a; Tiperman, A. Adsorption and Desorption of Stearic Acid Self-Assembled Monolayers on Aluminum Oxide. *Langmuir* **2007**, *23* (5), 2444–2452.

(15) Messerschmidt, C.; Schwartz, D. K. Growth Mechanisms of Octadecylphosphonic Acid Self-Assembled Monolayers on Sapphire (Corundum): Evidence for a Quasi-Equilibrium Triple Point. *Langmuir* **2001**, *17* (2), 462–467.

(16) Taylor, C. E.; Schwartz, D. K. Octadecanoic Acid Self-Assembled Monolayer Growth at Sapphire Surfaces. *Langmuir* **2003**, *19* (7), 2665–2672.

(17) Jeon, N. L.; Clem, P. G.; Nuzzo, R. G.; Payne, D. a. Patterning of Dielectric Oxide Thin Layers by Microcontact Printing of Self-Assembled Monolayers. *J. Mater. Res.* **1995**, *10* (12), 2996–2999.

(18) Kanaizuka, K.; Haruki, R.; Sakata, O.; Yoshimoto, M.; Akita, Y.; Kitagawe, H. Construction of Highly Oriented Crystalline Surface Coordination Polymers Composed of Copper Dithiooxamide Complexes. *J. Am. Chem. Soc.* **2008**, *130* (47), 15778–15779.

(19) Narita, A.; Baba, Y.; Sekiguchi, T.; Shimoyama, I.; Hirao, N.; Yaita, T. Anchoring of Alkyl Chain Molecules on Oxide Surface Using Silicon Alkoxide. *Appl. Surf. Sci.* **2012**, *258* (6), 2034–2037.

(20) Steinrück, H. G.; Magerl, A.; Deutsch, M.; Ocko, B. M. Pseudorotational Epitaxy of Self-Assembled Octadecyltrichlorosilane Monolayers on Sapphire (0001). *Phys. Rev. Lett.* **2014**, *113* (15), 1–6.

(21) Mitchon, L. L. N.; White, J. M. Growth and Analysis of Octadecylsiloxane Monolayers on Al2O3 (0001). *Langmuir* **2006**, *22* (15), 6549–6554.

(22) Piehler, J.; Brecht, A.; Geckeler, K. E.; Gauglitz, G. Surface Modification for Direct Immunoprobes. *Biosens. Bioelectron.* **1996**, *11* (6–7), 579–590.

(23) Brecht, A.; Gauglitz, G. Optical Probes and Tranducers. *Biosens. Bioelectron.* **1995**, *10*, 923–936.

(24) Brecht, A.; Gauglitz, G. Recent Developments in Optical Transducers for Chemical or Biochemical Applications. *Sensors Actuators B Chem.* **1997**, *38–39* (1–3), 1–7.

(25) Longo, G.; Szleifer, I. Ligand - Receptor Interactions in Tethered Polymer Layers. *Langmuir* **2005**, *21*, 11342–11351.

(26) Ren, C. L.; Carvajal, D.; Shull, K. R.; Szleifer, I. Streptavidin-Biotin Binding in the Presence of a Polymer Spacer. A Theoretical Description. *Langmuir* **2009**, *25* (20), 12283–12292.

(27) Mizaikoff, B. Waveguide-Enhanced Mid-Infrared Chem/bio Sensors. *Chem Soc Rev* **2013**, *42* (22), 8683–8699.

(28) Steinbach, A. M.; Sandner, T.; Mizaikoff, B.; Strehle, S. Gas Phase Silanization for Silicon Nanowire Sensors and Other Lab-on-a-Chip Systems. *Phys. Status Solidi C* **2016**, *13* (4), 135–141.

(29) Cras, J. J.; Rowe-Taitt, C. A.; Nivens, D. A.; Ligler, F. S. Comparison of Chemical Cleaning Methods of Glass in Preparation for Silanization. *Biosens. Bioelectron.* **1999**, *14* (8–9), 683–688.

(30) Kurth, D. G.; Bein, T. Surface Reactions on Thin Layers of Silane Coupling Agents. *Langmuir* **1993**, *9* (11), 2965–2973.

(31) Senkevich, J. J.; Yang, G. R.; Lu, T. M. Thermal Stability of Mercaptan Terminated Self-Assembled Multilayer Films on SiO2 Surfaces. *Colloids Surfaces A Physicochem. Eng. Asp.* **2002**, *207* (1–3), 139–145.

(32) Kattner, J.; Hoffmann, H. External Reflection Spectroscopy of Thin Films on Dielectric Substrates. In *Handbook of Vibrational Spectroscopy*; Chalmers, J. M., Griffiths, P. R., Eds.; J. Wiley & Sons: Chichester, 2002; Vol. 2, pp 1105–1123.

(33) Mielczarski, J. a. External Reflection Infrared-Spectroscopy At Metallic, Semiconductor, and Nonmetallic Substrates .1. Monolayer Films. *J. Phys. Chem.* **1993**, *97* (11), 2649–2663.

(34) Ishino, Y.; Ishida, H. Spectral Simulation of Uniaxially Oriented Monolayers in the Infrared. *Langmuir* **1988**, *4* (6), 1341–1346.

(35) Ramin, M. a.; Le Bourdon, G.; Daugey, N.; Bennetau, B.; Vellutini, L.; Buffeteau, T. PM-IRRAS Investigation of Self-Assembled Monolayers Grafted onto SiO2/Au Substrates. *Langmuir* **2011**, *27* (10), 6076–6084.

(36) Porter, M. D.; Bright, T. B.; Allara, D. L.; Chidsey, C. E. D. Spontaneously Organized Molecular Assemblies. 4. Structural Characterization of N-Alkyl Thiol Monolayers on Gold by Optical Ellipsometry, Infrared Spetcroscopy, and Electrochemistry. *J. Am. Chem. Soc.* **1987**, *109* (12), 3559–3568.

(37) Buontempo, J. T.; Rice, S. A. Infrared External Reflection Spectroscopy of Adsorbates on Dielectric Substrates : Determining Adsorbate Orientation in Langmuir Monolayers Infrared External Reflection Spectroscopy of Adsorbates on Dielectric Substrates : Determining Adsorbate Orientatio. *J. Chem. Phys.* **1993**, *98* (7), 5825–5834.

(38) Allara, D. L.; Nuzzo, R. G. Spontaneously Organized Molecular Assemblies. 2. Quantitative Infrared Spectroscopic Determination of Equilibrium Structures of Solution-Adsorbed N-Alkanoic Acids on an Oxidized Aluminum Surface. *Langmuir* **1985**, *1* (1), 52–66.

(39) Yen, Y.; Wong, J. S. Infrared Reflectance Properties of Surface Thin Films. *J. Phys. Chem.* **1989**, *93* (20), 7208–7216.

(40) Sangwan, M.; Stockwell, W. R.; Stewart, D.; Zhu, L. Absorption of Near UV Light by HNO 3 /NO 3 – on Sapphire Surfaces. *J. Phys. Chem. A* **2016**, *120* (3), 2877–2884.

(41) Dobrovinskaya, E. R.; Pishchik, V.; Lytvynov, L. A. *Sapphire: Material, Manufacturing, Applications*; Springer US, 2009.

(42) Mielczarski, J. A.; Mielczarski, E. Determination of Molecular Orientation and Thickness of Self-Assembled Monolayers of Oleate on Apatite by FTIR Reflection Spectroscopy. *J. Phys. Chem.* **1995**, *99* (10), 3206–3217.

(43) Rotole, J. A.; Sherwood, P. M. A. Valence Band X-Ray Photoelectron Spectroscopic Studies to Distinguish between Oxidized Aluminum Species. *J. Vaccum Sci. Technol.* **1999**, *17* (4), 1091–1096.

(44) Sherwood, P. M. A. Introduction to Studies of Aluminum and Its Compounds by XPS. *Surf. Sci. Spectra* **1998**, *5* (1), 1–3.

(45) Stacchiola, D.; Kaya, S.; Weissenrieder, J.; Kuhlenbeck, H.; Shaikhutdinov, S.; Freund, H. J.; Sierka, M.; Todorova, T. K.; Sauer, J. Synthesis and Structure of Ultrathin Aluminosilicate Films. *Angew. Chemie - Int. Ed.* **2006**, *45* (45), 7636–7639.

(46) Todea, M.; Vanea, E.; Bran, S.; Berce, P.; Simon, S. XPS Analysis of Aluminosilicate Microspheres Bioactivity Tested in Vitro. *Appl. Surf. Sci.* **2013**, *270*, 777–783.

(47) Simon, V.; Cavalu, S.; Simon, S.; Mocuta, H.; Vanea, E.; Prinz, M.; Neumann, M. Surface Functionalisation of Sol-Gel Derived Aluminosilicates in Simulated Body Fluids. *Solid State Ionics* **2009**, *180* (9–10), 764–769.

(48) Hu, M.; Noda, S.; Okubo, T.; Yamaguchi, Y. Structure and Morphology of Self-Assembled Layers on Silicon Oxide. *Appl. Surf. Sci.* **2001**, *181*, 307–316.

(49) Liu, J.; Hlady, V. Chemical Pattern on Silica Surface Prepared by UV Irradiation of 3-Mercaptopropyltriethoxy Silane Layer: Surface Characterization and Fibrinogen Adsorption. *Colloids Surfaces B Biointerfaces* **1996**, *8* (1–2), 25–37.

(50) Yu, Y.; Addai-Mensah, J.; Losic, D. Chemical Functionalization of Diatom Silica Microparticles for Adsorption of Gold (III) Ions. *J Nanosci Nanotechnol* **2011**, *11* (12), 10349–10356.

(51) Pensa, E.; Corte, E.; Fonticelli, M. H.; Benítez, G.; Rubert, A.; Salvarezza, R. C. The Chemistry of the Sulfur- Gold Interface : In Search of a Unified Model. *Acc. Chem. Res.* **2012**, *45* (8), 1183–1192.

(52) Gronbeck, H.; Curioni, A.; Andreoni, W. Thiols and Disulfides on the Au (111) Surface: The Headgroup - Gold Interaction. *J. Am. Chem. Soc.* **2000**, *122* (16), 3839–3842.

(53) Jabarullah, N. H.; Verrelli, E.; Mauldin, C.; Navarro, L. A.; Golden, J. H.; Madianos, L. M.; Kemp, N. T. Superhydrophobic SAM Modified Electrodes for Enhanced Current Limiting Properties in Intrinsic Conducting Polymer Surge Protection Devices. *Langmuir* **2015**, *31* (22), 6253–6264.

(54) Kranz, C.; Kueng, A.; Lugstein, A.; Bertagnolli, E.; Mizaikoff, B. Mapping of Enzyme Activity by Detection of Enzymatic Products during AFM Imaging with Integrated SECM-AFM Probes. *Ultramicroscopy* **2004**, *100* (3–4), 127–134.

(55) Pavlovic, E.; Quist, A. P.; Gelius, U.; Oscarsson, S. Surface Functionalization of Silicon Oxide at Room Temperature and Atmospheric Pressure. *J. Colloid Interface Sci.* **2002**, *254* (1), 200–203.

(56) Ptak, A.; Gojzewski, H.; Kappl, M.; Butt, H. J. Quantitative Analysis of the Interaction between an Atomic Force Microscopy Tip and a Hydrophobic Monolayer. *J. Phys. Chem. C* **2010**, *114* (49), 21572–21578.

(57) Kondo, T.; Yanagida, M.; Shimazu, K.; Uosaki, K. Determination of Thickness of a Self-Assembled Monolayer of Dodecanethiol on Au(111) by Angle-Resolved X-Ray Photoelectron Spectroscopy. *Langmuir* **1998**, *14* (19), 5656–5658.

(58) Verwey, E. J. W.; Overbeek, J. T. G. *Theory of the Stability of Lyophobic Colloids*; Elsevier Publishing Company: Eindhoven, 1948.

(59) Duval, J. F. L.; Leermakers, F. A. M.; Leeuwen, H. P. Van. Electrostatic Interactions between Double Layers: Influcence of Surface Roughness, Regulation, and Chemical Heterogeneities. *Langmuir* **2004**, *20* (12), 5052–5065.

For TOC only

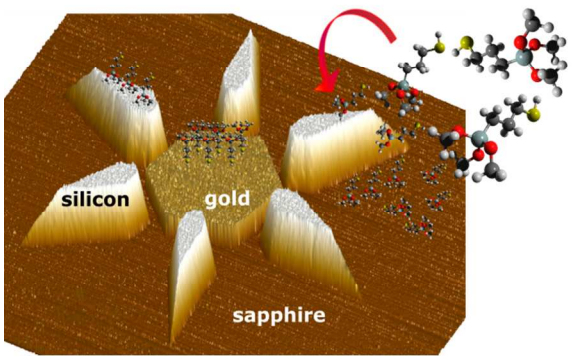
silicon
gold
sapphire

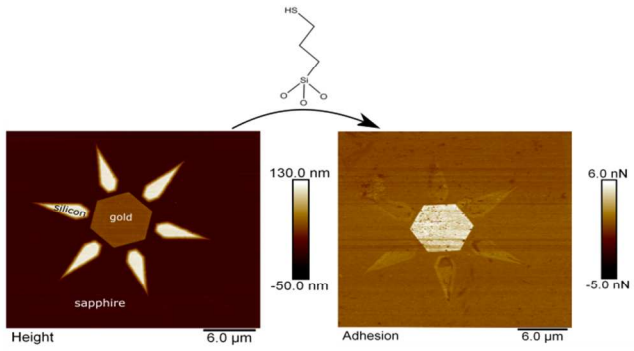
HS
Si
O
O
O
silicon
gold
sapphire
130.0 nm
-50.0 nm
Height
6.0 µm
6.0 nN
-5.0 nN
Adhesion
6.0 µm